RSC Advances

Low temperature and controlled synthesis of Bi2(S1-xSex)3 thin films using simple chemical route:Effect of bath composition

Journal:	*RSC Advances*
Manuscript ID:	RA-ART-04-2015-007372.R1
Article Type:	Paper
Date Submitted by the Author:	04-Jun-2015
Complete List of Authors:	Salunkhe, Manauti; Defence Institute of Advance Technology, Department of Applied Physics Khot, Kishorkumar; Shivaji University, Department of Chemistry Sahare, Sanjay; Defence Institute of Advance Technology, Department of Applied Physics Bhosale, Popatrao; Shivaji University, Chemistry; Bhave, Tejashree; Defence Institute of Advanced Technology, Applied Physics

Journal Name

ARTICLE

Low temperature and controlled synthesis of $Bi_2(S_{1-x}Se_x)_3$ thin films using simple chemical route: Effect of bath composition

Received 00th January 20xx,
Accepted 00th January 20xx

DOI: 10.1039/x0xx00000x

www.rsc.org/

Manauti M. Salunkhe[a], Kishorkumar V. Khot[b], Sanjay H. Sahare[a], Popatrao N. Bhosale[b] and Tejashree Bhave[a*]

Nanostructured Bismuth sulphoselenide ($Bi_2(S_{1-x}Se_x)_3$) thin films have been synthesized using a simple, cost-effective chemical bath deposition (CBD) method at room temperature (300K). Structural, compositional, morphological, optical characterization and the photoelectrochemical performance testing of these $Bi_2(S_{1-x}Se_x)_3$ thin films has been carried out. The X-ray diffraction (XRD) study demonstrates that these thin films are nanocrystalline in nature with pure orthorhombic crystal structure. An X-ray photoelectron spectroscopy (XPS) and energy dispersive X-ray spectroscopy (EDS) show that the deposited thin films are nearly stoichiometric in nature. Field emission scanning electron microscopy (FESEM) reveals different morphologies for $Bi_2(S_{1-x}Se_x)_3$ thin films. Linear nature of plots seen in UV-Vis-NIR absorption study confirms direct allowed type of transition. *J-V* measurements with solar simulator were carried out for all samples and the highest photoconversion efficiency 0.3845% has been recorded for Bi_2Se_3 thin film. Significant boost in photoelectrochemical (PEC) performance might be due to the larger surface area with lower dislocation density and micro strain with lower level of grain boundaries resistance of Bi_2Se_3 thin films.

1. Introduction

Thin film-based PEC solar cells have wide applications due to their low fabrication cost, high throughput processing techniques and ease of junction formation with an electrolyte.[1,2] Therefore, PEC solar cells with semiconductor under investigation can be used as a simple and rapid technique to test the quality of solar cell materials. Also, the choice of semiconductor which facilitates effective charge transfer processes at the semiconductor/electrolyte interface is very important in development of any PEC cell. Semiconductor material for this application must have a band gap energy in between 1.0 and 3.0 eV in order to utilize most part of the visible region of solar spectrum and should be highly stable against corrosion.[3-5]

Interest in the use of photoelectrochemical (PEC) solar cells based on thin-film semiconductor photoelectrodes arises because of low cost of fabrication and possibility of obtaining larger-area solar cells. Presently, nanocrystalline materials have applications in the field of electronic applications, since the material properties could be changed by changing the crystallite size and thickness of film. Development of such materials, whose structural, morphological and optical properties could be controlled, will be useful in many ways. For example, optoelectronic devices, particularly solar energy conversion devices could be modified accordingly.[6] Group V–VI semiconductors with energy gaps covering the visible spectral range are promising candidates for PECs.[7,8] Bi_2S_3 and Bi_2Se_3 are two very important wide gap semiconductors because of their applications in optoelectronics and PEC.[9,10] Ternary V-VI group semiconductors such as $Bi_2(SSe)_3$, $Bi_2(Te_{0.5}Se_{0.5})_3$ and $Bi_2(S_{1-x}Te_x)_3$ have been reported.[11-13] The alloy of BiSSe can have promising applications since its band gap can be tuned by means of the composition in between ~1.92 eV (for Bi_2S_3) and ~ 1.40 eV (for Bi_2Se_3), almost covering the entire visible range.

Considering the advantages laid down by ternary alloy thin films, in present report, our key focus is to investigate the properties of $Bi_2(S_{1-x}Se_x)_3$ thin films using facile CBD technique at room temperature. Chemical bath deposition technique is used to deposit $Bi_2(S_{1-x}Se_x)_3$ thin films without use of any toxic reagents, solvent etc. Also room temperature CBD has prospective advantages such as large scale deposition, low temperature deposition process, possibility to use conducting as well as non-conducting substrates for deposition, reproducibility and most significantly no requirement of highly sophisticated equipment. All films were synthesized simply by keeping the reaction bath at room temperature (300K) for 4h. Such techniques already have been used to deposit $MoBi_2S_5$ films for PEC solar cell applications. Pawar N.B. et.al.[14] (2012) have reported efficiency of 0.048% for as deposited MoBi2S5 film and 0.078% after surfactant treatment. Further many people have changed the composition and stoichiometry of

[a] aThin Film Material Laboratory, Department of Applied Physics,
[b] Defense Institute of Advance Technology (DU), Girinagar, Pune-411025, India
[c] bMaterials Research Laboratory, Department of Chemistry, Shivaji University, Kolhapur-416004, India.
[d] Corresponding author : tejashreebhave@diat.ac.in (Tejashree Bhave)
[e] Tel: +91 20 2430 4093; Fax: +91 20 2438950

chalcogenides to achieve the efficiency up to 0.1%[15,16]. Here, in comparison to other reports[17], we have tried to study the efficiency change with the Sulphite (S) and Selenide (Se) concentration in Bismuth (Bi). Structural, compositional, morphological, optical properties and their PEC behavior of all thin films were studied and discussed in detailed in this report.

2. Experimental

2.1 Materials and Methods

All chemicals were of analytical reagent (AR) grade and used without further purification. Bismuth Nitrate ($Bi(NO_3)_3 5H_2O$) (99 %, S-D Fine Chem.), Thioacetamide (C_2H_5NS) (99% pure, S-D Fine Chem.), Selenium metal powder (99.5%, Sigma Aldrich), Sodium Sulphite (Na_2SO_3) (96%, S-D Fine Chem.), Liquor Ammonia (NH_3), (28-30% Thomas Baker) and Triethanolamine (TEA) ($N(CH_2\text{-}CH_2\text{-}OH)_3$), (99% Merck) were used as precursors and complexing agents. For measurement of photoelctrochemical cell properties, we used iodite/polyiodite (I^-/I_3^-) redox electrolyte prepared from Lithium Iodide (LiI) (99.9%, Sigma Aldrich), Iodite (I_2) (99.8%, Sigma Aldrich) and Anhydrous Ethylene Glycol ($C_2H_6O_2$) (99.8%, Sigma Aldrich). Substrates were ultrasonically cleaned by using detergent followed by methanol treatment and finally cleaned with acetone and deionized water. $Bi_2(S_{1-x}Se_x)_3$ thin films were deposited on to ultrasonically cleaned glass as well as FTO-coated glass substrates by using Simple CBD technique at room temperature.

2.2 Deposition of $Bi_2(S_{1-x}Se_x)_3$ thin films

In room temperature CBD synthesis Bi-TEA complex react with S^{2-} and Se^{2-} chalcogen ions, which are released slowly from dissociation of $CH_3\text{-}CS\text{-}NH_2$ and Na_2SeSO_3 at alkaline pH 9.7. Solution of 0.05M Bi-TEA complex was used as a source of Bi^{3+} ions, where bismuth nitrate was triturated with TEA as complexing agent for 8 hrs. Sodium selenosulfite (Na_2SeSO_3) was prepared by refluxing selenium metal powder with anhydrous sodium sulfite at 90˚ for 8 hrs.

Nucleation and thin film formation in CBD is mainly dependent on different preparative parameters such as, complexing agent, precursor concentration, pH, deposition time and temperature of bath. These parameters were optimized during the initial stage of thin film deposition. The concentration of Bi-TEA complex was kept constant for all compositions. The concentration of $CH_3\text{-}CS\text{-}NH_2$ and Na_2SeSO_3 were varied in a volume stoichiometric ratio so as to obtain various compositions of $Bi_2(S_{1-x}Se_x)_3$ thin films. The deposited films were designated as BS1, BS2, BS3, BS4 and BS5 for x = 0, 0.3, 0.5, 0.7 and 1 respectively.

2.3 Characterization of thin films

Thickness of deposited thin films was measured by using surface profiler (AMBIOS XP-1). Structural properties were confirmed by using X-ray diffractometer (Bruker AXS, D8) using Cu Kα (λ =1.5418 Å) radiation for 2θ ranging from 20º to 70º. Elemental information concerning to as-deposited $Bi_2(S_{1-x}Se_x)_3$ thin films was characterized by using an X-ray photoelectron spectrometer (XPS, Thermo Scientific, Multilab-2000) with a multi-channel detector, which can endure high photon energies from 0.1-3.0 KeV. Surface morphology and elemental composition of as-deposited thin films were investigated using field emission scanning electron microscopy (FESEM) equipped with energy dispersive X-ray spectroscopy (EDS) analyzer (Hitachi, S-4700). Topography and roughness of films were measured by using Asylum Research MFP3D atomic force microscopy (AFM). Optical absorption spectra were recorded using UV-Vis spectrophotometer (Shimadzu, UV-1800). PEC measurements were carried out using semiconductor parameter analyzer (Keithley SCS-4200 Semiconductor) characterization unit using 500 W tungsten filament lamp (Intensity 30 mW/cm^2) in iodite/polyioditeredox electrolyte. PEC cell was fabricated using standard two electrode configuration, comprising glass-FTO/$Bi_2(S_{1-x}Se_x)_3$ (active surface area of 1 cm^2) photoelectrode, and graphite as counter electrode. All measurements were done at room temperature (300K) in air.

3. Results and Discussion

3.1 Growth and reaction mechanism of thin film formation

Precipitation of metal chalcogenide thin films in chemical bath deposition technique occurs only when the ionic product of ions (both anion and cation) exceeds the solubility product of metal chalcogenides.[18] Usually ions combine to form nuclei on the substrate as well as in the solution, and precipitation occurs. The film growth takes place by means of ion-by-ion condensation of material or by adsorption of colloidal particles from the solution on the substrate. Slow release of metal ions can be achieved by using chelating agents which helps to control the reaction rate in CBD. Generally, a slow reaction rate results in adherent and good quality thin film formation.

The formation of $Bi_2(S_{1-x}Se_x)_3$thin films using TEA as complexing agent proceeds via following reaction (equation 1),

$$\underset{\text{Bi-TEA Complex}}{2[Bi\,N\,(CH_2\text{-}CH_2\text{-}O)_3]} + \underset{\text{Thioacetamide}}{nH_3C\text{-}\overset{\overset{S}{||}}{C}\text{-}NH_2} + \underset{\text{Sodium Selenosulphite}}{nNa_2SeSO_3} + nOH^- \xrightarrow[\text{R.T.}]{\text{pH 9.7}} [Bi_2(S_{1-x}Se_x)_3] + nNa_2SO_4 + \underset{\underset{O}{||}}{nH_3C\text{-}C\text{-}NH_2} + \underset{\text{TEA}}{2[N(CH_2CH_2\text{-}OH)_3]} \quad [1]$$

The formation of $Bi_2(S_{1-x}Se_x)_3$thin films using TEA as complex agent proceeds via following reaction (equation 1),
TEA is stable throughout the deposition time. Initially slow release of Bi^{3+}, S^{2-} and Se^{2-} ions from Bi-TEA, CH3-CS-NH_2 and Na_2SeSO_3 complex takes place at alkaline pH 9.7 at room temperature. Released Bi^{3+}, S^{2-} and Se^{2-} ions starts to condense on the substrate surface in the order to form a number of small nuclei through a multi nucleation process. When the ionic product of Bi^{3+}, S^{2-} and Se^{2-} ions exceeds the solubility product of $Bi_2(S_{1-x}Se_x)_3$, a heterogeneous reaction starts which leads to the slow deposition of a $Bi_2(S_{1-x}Se_x)_3$ thin films on the substrate surface. Further growth results in formation of nanostructured $Bi_2(S_{1-x}Se_x)_3$ thin films. A possible growth mechanism for the deposition of nanostructured $Bi_2(S_{1-x}Se_x)_3$ thin films is shown in fig. 1.

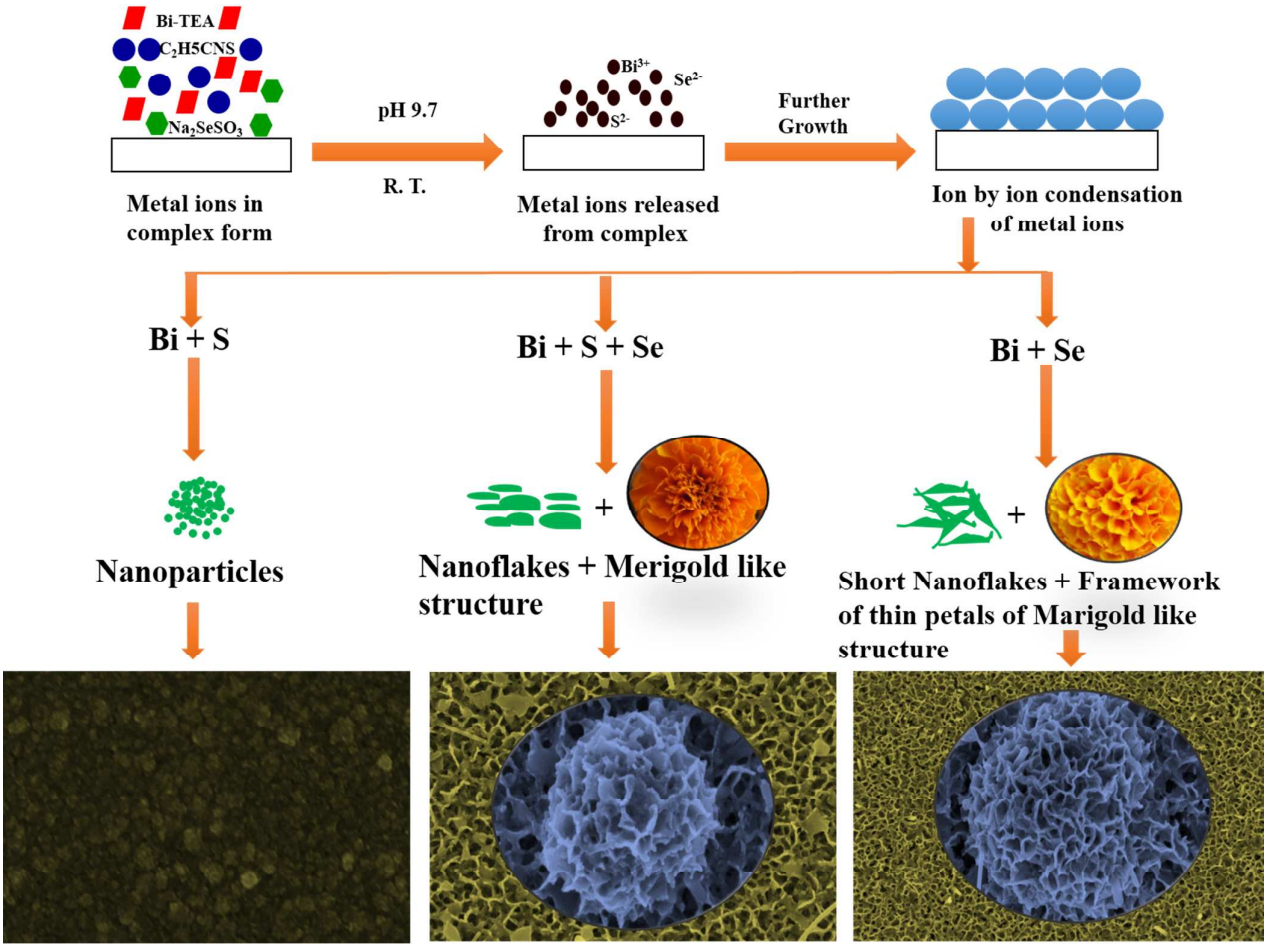

Fig. 1 Comprehensive growth mechanism of $Bi_2(S_{1-x}Se_x)_3$thin films

3.2 Structural Studies

Crystal quality and structural analysis was carried out by using X-ray diffraction pattern in range of 2θ = 20˚ to 70˚. Fig. 2 shows X-ray diffraction patterns of $Bi_2(S_{1-x}Se_x)_3$ thin films. The major diffraction peaks in BS1 thin film sample are centered at 2θ = 24.86˚, 26.55˚, 30.21˚, 33.07˚, 36.07˚, 41.03˚, 43.90˚, 47.03˚, 54.07˚, 60.07˚ and 66.20˚ which can be indexed to the (110), (031), (121), (041), (123), (051), (052), (151), (116), (072) and (172) crystal planes respectively. Also the major diffraction peaks of sample BS5 centered at 2θ = 25.12˚, 32.68˚, 34.11˚, 41.16˚, 45.07˚, 47.81˚, 54.47˚, 56.94˚, 58.25˚, 67.12˚ and 69.21˚ which can be indexed to the (120), (220), (101), (211), (221), (140), (231), (041), (340), (440) and (151) crystal planes respectively. The major diffraction peaks of sample BS2 to BS4 ($Bi_2(SSe)_3$) centered at 2θ (Bi_2S_3) = 24.37˚, 33.84˚, 42.31˚ and 54.79˚ can be indexed to the (013), (130), (051) and (036) crystal planes respectively and 2θ (Bi_2Se_3) =. 25.52˚, 30.70˚, 44.61˚, 48.19˚ and 57.66˚ can be indexed to the (021), (221), (151), (620) and (422) crystal planes respectively. These plane indices are obtained by comparing the intensities and positions of peaks with those of Bi_2S_3 and Bi_2Se_3 phases. This clearly is an indication of a mixed phase formation in the sample BS2 to BS4.
All diffraction peaks in the XRD patterns could be indexed to the orthorhombic crystal structure of Bi_2S_3 and Bi_2Se_3 which

are in good agreement with the standard data for Bi_2S_3 (JCPDS data file no 84-0279) and Bi_2Se_3 (JCPDS data file no 77-2016). Sample BS1 and BS5 show single phase formation of Bi2S3 and Bi2Se3 thin films respectively those are shown by vertical lines in fig.2 (BS1 and BS5). Sample BS2 to BS4 shows mix phase formation of (●) Bi_2S_3 and (■) Bi_2Se_3 which is shown in fig. 2 (BS2 to BS4).

The broad and intense diffraction peaks in XRD pattern confirm that the samples are nanocrystalline in nature without any amorphous component.[19] No other unassigned peaks were observed, which in turn shows that material is in pure phase.

Further, average crystallite size was calculated by using Scherrer formula[20] (equation 2), dislocation density (δ) and micro strain (ε) for all samples were determined by using equations (equation 3 and 4)[21] and are summarized in Table 1;

$$\mathbf{D} = \frac{\mathbf{0.94\lambda}}{\boldsymbol{\beta}\mathbf{COS\theta}} \qquad [2]$$

where, D is average crystallite size, λ is wavelength of X-ray radiation (1.5406 Å), β is full width at half maximum (FWHM) in radians and θ is Bragg's angle. Calculated average crystallite size increases from 35.7 to 97.5 nm for BS1 to BS5 respectively. This enhancement in average crystallite size is beneficial for improvement of photon conversion efficiency.[22,23]

$$\boldsymbol{\delta} = \left(\frac{\mathbf{1}}{\boldsymbol{D}^2}\right) \qquad [3]$$

$$\boldsymbol{\varepsilon} = \left(\frac{\boldsymbol{\beta}\,\mathbf{cot\theta}}{\mathbf{4}}\right) \qquad [4]$$

Enhancement in crystallite size as well as reduction in dislocation density (δ) and micro strain (ε) was observed with increase in selenium content in the films (BS1 to BS5) as can be seen from Table 1[24,25]. Decrease in δ and ε indicates lower level of lattice imperfections[26] and formation of high quality $Bi_2(S_{1-x}Se_x)_3$ thin films.

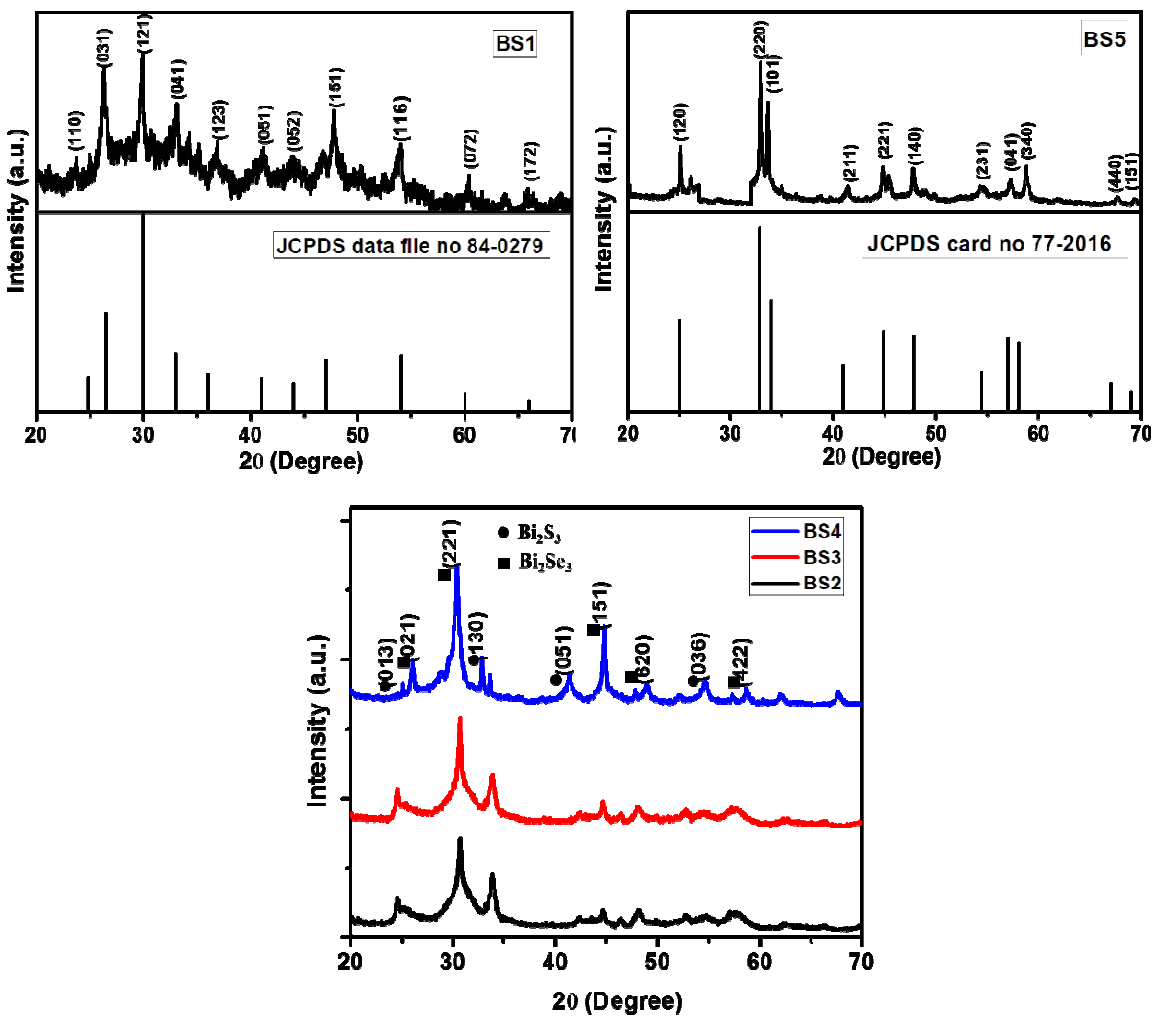

Fig. 2 X-ray diffraction patterns of $Bi_2(S_{1-x}Se_x)_3$(BS1 to BS5) thin films.

Table 1 Statistics of the thickness, optical band gap (Eg), crystallitesize (D), dislocation density (δ) and micro-strain (ε) of $Bi_2(S_{1-x}Se_x)_3$ thin films.

Sample code	Thickness (nm)	Band Gap (Eg) eV	Crystallite Size (D) (nm)	Dislocation density (δ) × 10^{-3} lines m^{-2}	Microstrain (ε)
BS1	312	1.69	35.7	0.801	0.524
BS2	350	1.62	40.1	0.628	0.452
BS3	388	1.57	56.5	0.313	0.254
BS4	420	1.51	79.2	0.159	0.155
BS5	469	1.43	97.5	0.105	0.101

3.3 Compositional studies

3.3.1 X-ray photoelectron spectroscopy

XPS analysis was carried out to confirm composition of BS1, BS3 and BS5 thin films as shown in fig. 3. Typical XPS survey spectrum (fig.3 (a)) recorded for BS1 film indicates the presence of Bismuth (Bi), Sulphur (S), Carbon (C) and Oxygen (O) elements. Carbon correction was carried out before analyzing high resolution core level spectra's. High resolution core level spectrum for Bi (4f) is shown in (fig. 3 (b)) recorded for BS1 film. The two peaks in Bi (4f) core level spectrum arise with Bi4f5/2 peak position at the 163.7 eV and Bi4f7/2 at 158.8 eV binding energies respectively. S (2p) spectrum (fig.3 (c)) recorded for BS1 film shows two relevant peaks for S2p1/2 peak positions at 161.8 and S2p3/2 at 160.3 eV binding energies respectively. Typical XPS survey spectrum (fig.3 (d)) recorded for BS3 thin film indicates the presence of Bi, S, Se, C and O elements. High resolution core level spectrum of Bi(4f) is shown in (fig. 3 (e)) recorded for BS3 thin film. Two peaks in Bi(4f) core level spectrum arises with Bi4f5/2 peak position at 164.1 eV and Bi4f7/2 arises at 159.2 eV binding energies respectively. S (2p) spectrum (fig. 3 (f)) BS3 thin film shows two relevant peaks for S2p1/2 peak position at 161.7 eV and S2p3/2 arises at 160.4 eV binding energies respectively. Se (3d) core level spectrum (fig.3 (g)) recorded for BS3 shows two relevant peaks for Se3d3/2 peak position at 54.9eV and Se3d5/2 arises at 53.8 eV binding energies respectively. Typical XPS survey spectrum (fig. 3 (h)) recorded for BS5 thin film indicates the presence of Bi, and Se, elements. High resolution core level spectrum of Bi(4f) is shown in (fig.3 (i)) recorded for BS5 thin film. The two peaks in Bi (4f) core level spectrum arise with Bi4f5/2 peak position at 163.3 and Bi4f7/2 arises at 158.2 binding energies respectively. Se (3d) spectrum (fig. 3 (j)) recorded for BS5 thin film shows two relevant peaks at Se3d3/2 peak position at 55.9 eV and Se3d5/2 arises at 53.4 eV binding energies respectively. The values of binding energies for Bi, S and Se are at respective positions for Bi^{3+}, S^{2-} and Se^{2-} states. These results confirm the composition of the films.

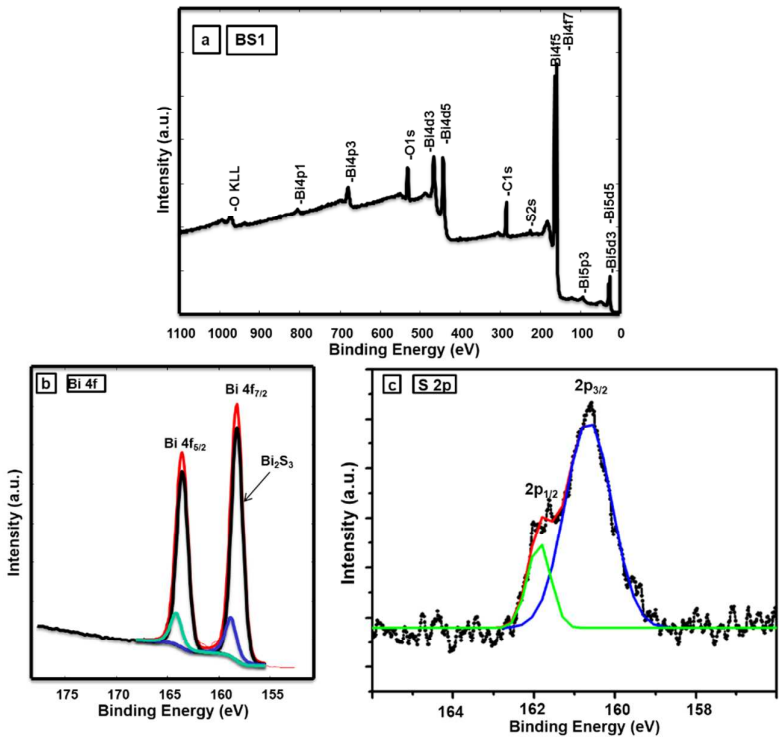

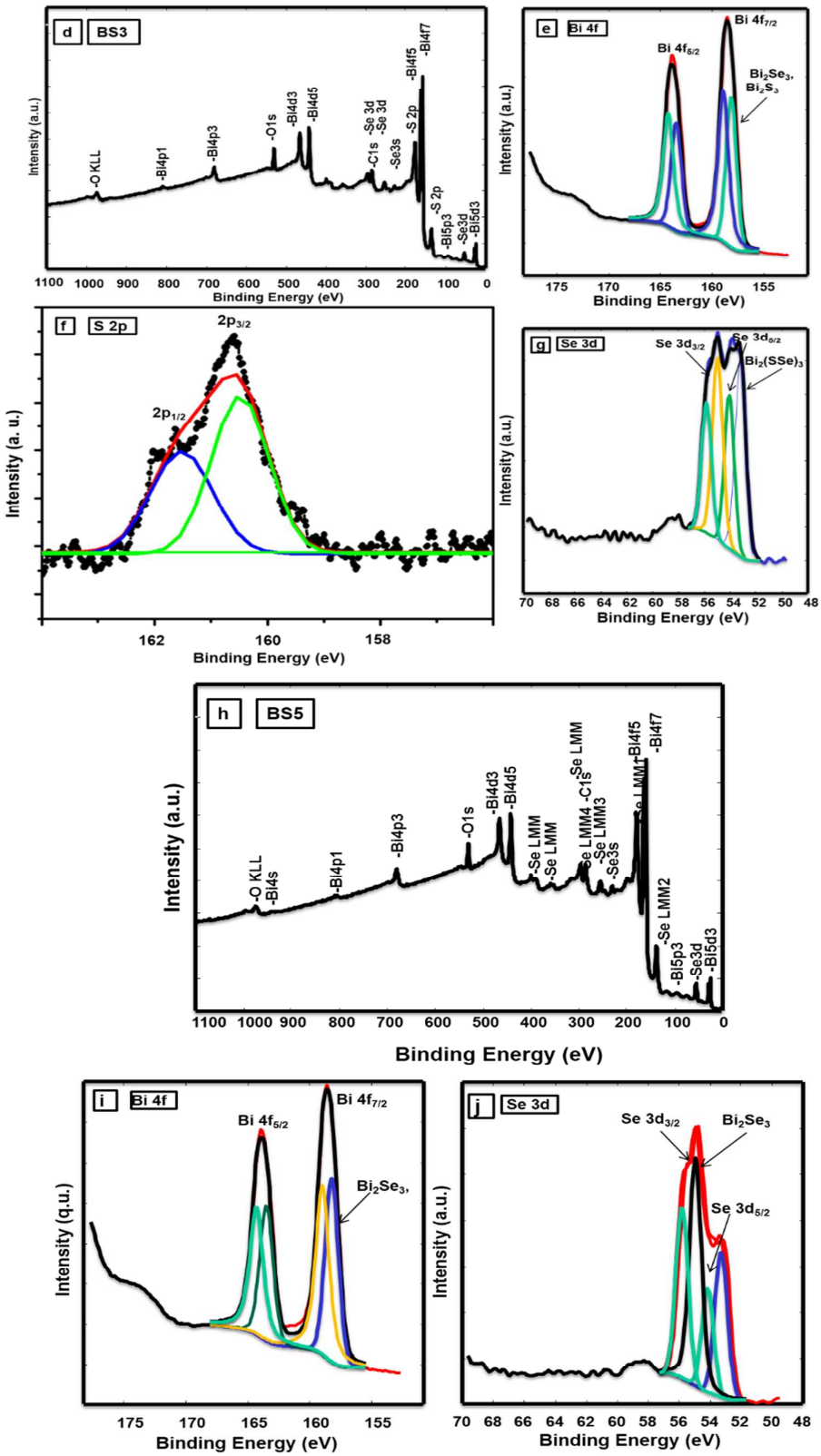

Fig. 3 Fig. 3 a) Survey spectrum of BS1 b) Core level spectrum of Bi4f in BS1 c) Core level spectrum of S2p in BS1 d) Survey spectrum of BS3 e) Core level spectrum of Bi4f in BS3 f) Core level spectrum of S2p in BS3 g) Core level spectrum of Se 3d in BS3 h) Survey spectrum of BS5 i) Core level spectrum of Bi4f in BS5 j) Core level spectrum of Se3d in BS5

3.3.2 Energy dispersive X-ray spectroscopy

Quantitative analysis was carried out to confirm the atomic percentage of Bi, S and Se in deposited thin film using EDS technique. Fig.4 indicates representative EDS spectra of typical BS1, BS3 and BS5 thin films. Fig.4 BS1, BS3 and BS5 which confirms the presence of Bi, S and Se elements. Inset of fig.4 (BS1, BS3 and BS5) shows tabulated data of expected and actual atomic percentage for Bi, S and Se elements. From these tables we can clearly see that actual atomic percentage of elements is in well agreement with expected atomic percentage. Thus the formation of Bi_2S_3, $Bi_2(S_{0.5}Se_{0.5})_5$ and Bi_2Se_3 is confirmed. The small amount of deviation of actual atomic percentage from expected atomic percentage of Bi, S and Se elements can be due to trace inclusion of oxygen in to the films from atmospheric contaminations and during transfer of films as well as the variation of bismuth due to the antisite defect.[27,28]

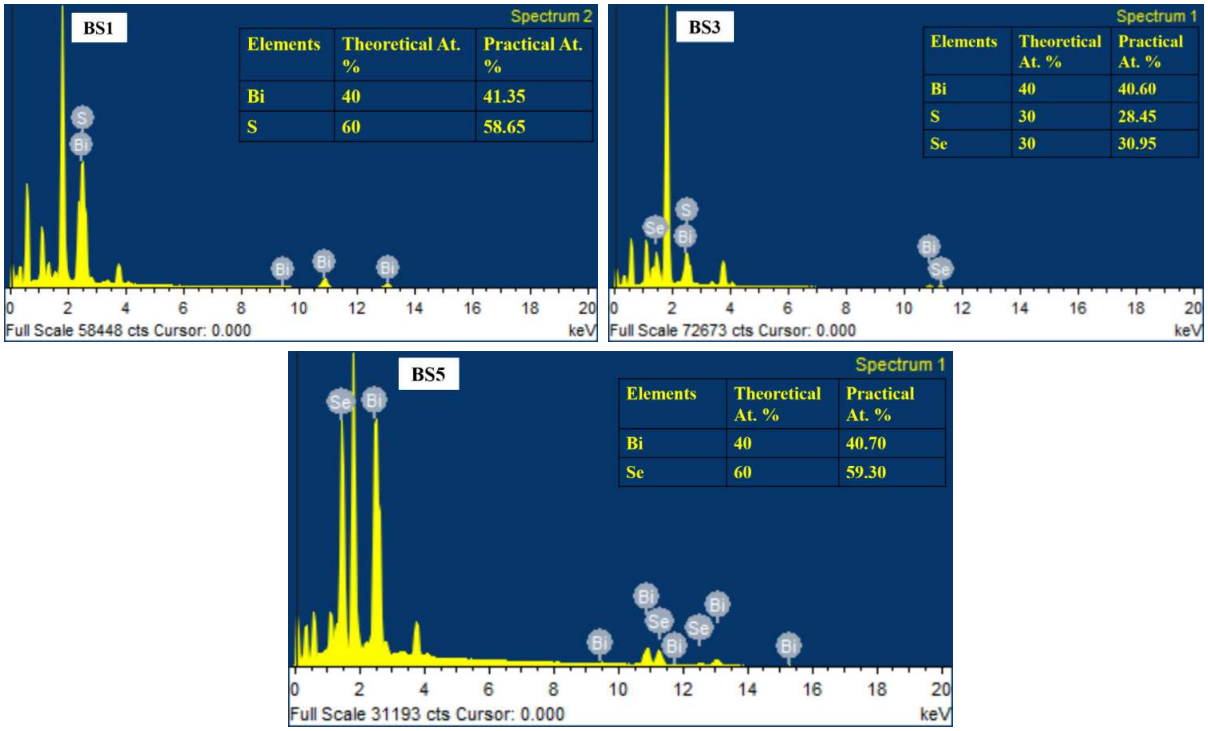

Fig. 4 EDS Spectrum of $Bi_2(S_{1-x}Se_x)_3$thin films

3.4 Morphological studies

3.4.1 Field emission scanning electron microscopy

FESEM analysis was carried out to study the surface morphology of $Bi_2(S_{1-x}Se_x)_3$ thin films (BS1 to BS5) at different magnifications as shown in fig. 5. High magnification FESEM image of fig.5 (BS1) reveals that the Bi_2S_3 thin films exhibit a uniform pin hole free morphology consisting of tightly packed nanoparticles. After addition of appropriate amount of selenium in binary bismuth sulphide, a porous film containing nanosized flakes as well as nanoflowers which have structure like a marigold bud is observed in (fig.5 (BS2 a,b,c)). It seems that this marigold like structure is formed as additional layers are added causing the flakes to branch out from one another. In $Bi_2(S_{1-x}Se_x)_3$ thin films, (fig. 5 (BS3 a,b,c)) when sulphur and selenium are in equal quantity, a porous film with combined structure of nanoflakes and nanoflowers is observed. However we can see that the petals in this nanoflower are more open and separate due to further branching out of nanoflakes. When selenium is in high quantity and sulpher is at low quantity in $Bi_2(S_{1-x}Se_x)_3$ thin films, (fig. 5 (BS4 a,b,c)) we again observed a porous film with nanoflakes and nanoflowers. However we can see that the spatial separation of petals in the nanoflower has further increased. For Bi_2Se_3 thin films, (fig. 5 (BS5 a,b,c)) we observed increase in pore size as well as short nanoflakes, still further increase in size of nanoflowers and number of petals along with clearly observable reduction between separation of petals in the flower. Quantitative analysis of these observations has been presented in Table 2. It can be clearly seen that, as the percentage of Se in the films increases, pore size, number of petals in the nanoflowers and consequently surface area goes on increasing. Generally semiconductor films with porous structure have exhibited improved performance of solar cells[29] due to the large surface area to reduce the e^-/h^+ recombination transfer. Thus it appears that the enhanced PEC property of Bi_2Se_3 originates not only from the increased optical absorption but also as a consequence of porous nature.[30, 31]

Journal Name

ARTICLE

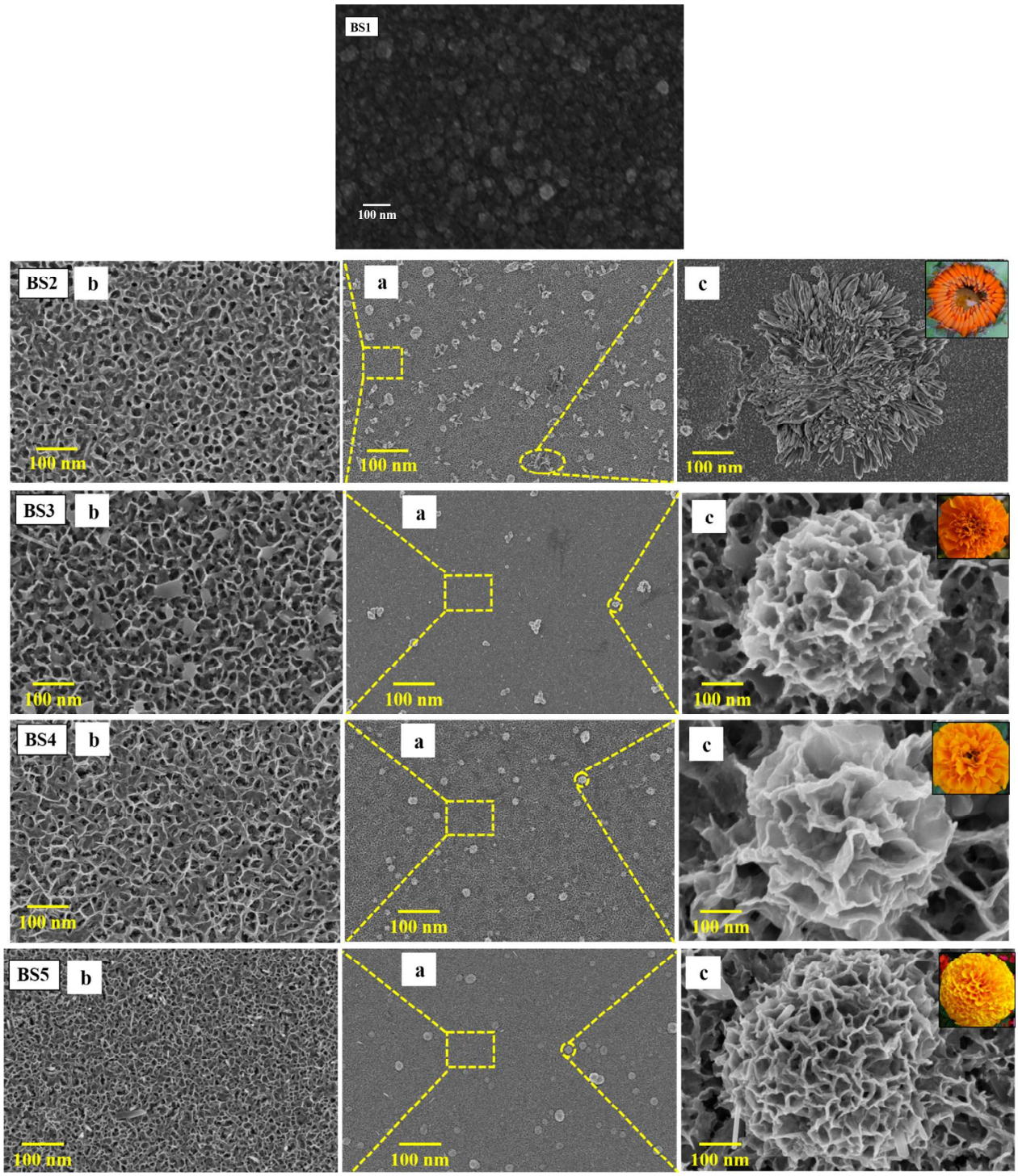

Fig. 5 Field emission scanning electron microscopy (FESEM) micrographs of $Bi_2(S_{1-x}Se_x)_3$(BS1 to BS5) thin films

Table 2 Statistics of the flower size, pore size, nanoflakes wall thickness, size of petal, size of nanoflex of $Bi_2(S_{1-x}Se_x)_3$ thin films.

Sample code	Flower size (μm)	Pore size (nm)	Wall thickness of nanoflakes (nm)	Size of petals (nm)	Size of nanoflakes (nm)
BS1	-	-	-	-	-
BS2	1.102	205.8	57.32	109.2	263.8
BS3	1.289	241.4	32.46	146.6	210.3
BS4	1.527	279.6	25.15	263.8	175.8
BS5	1.859	295.6	14.75	189.2	125.7

3.4.2 Atomic force microscopy

Surface roughness of $Bi_2(S_{1-x}Se_x)_3$ thin films (BS1 to BS5) were recorded by AFM. Fig.6 shows typical two dimensional (2D) (Fig 6(a)) and (b) three dimensional (3D) (Fig. 6(b)) AFM images of $Bi_2(S_{1-x}Se_x)_3$ thin films (BS1 to BS5) respectively. From all AFM images it is confirmed that all thin films are uniform, without cracks and well-adherent to the substrate. These results are consistent with observed SEM results. Roughness values of 1.17, 1.57, 1.89, 2.27 and 2.52nm have been measured for BS1, BS2, BS3, BS4 and BS5 thin films respectively. In 3D images the intensity strip indicates the height of surface grains along z axis. Such improvement in surface roughness is highly beneficial for solar cell application, because such rough surfaces may provide more light scattering and light trapping phenomenon, which is highlighted on overall photo conversion efficiency of material.

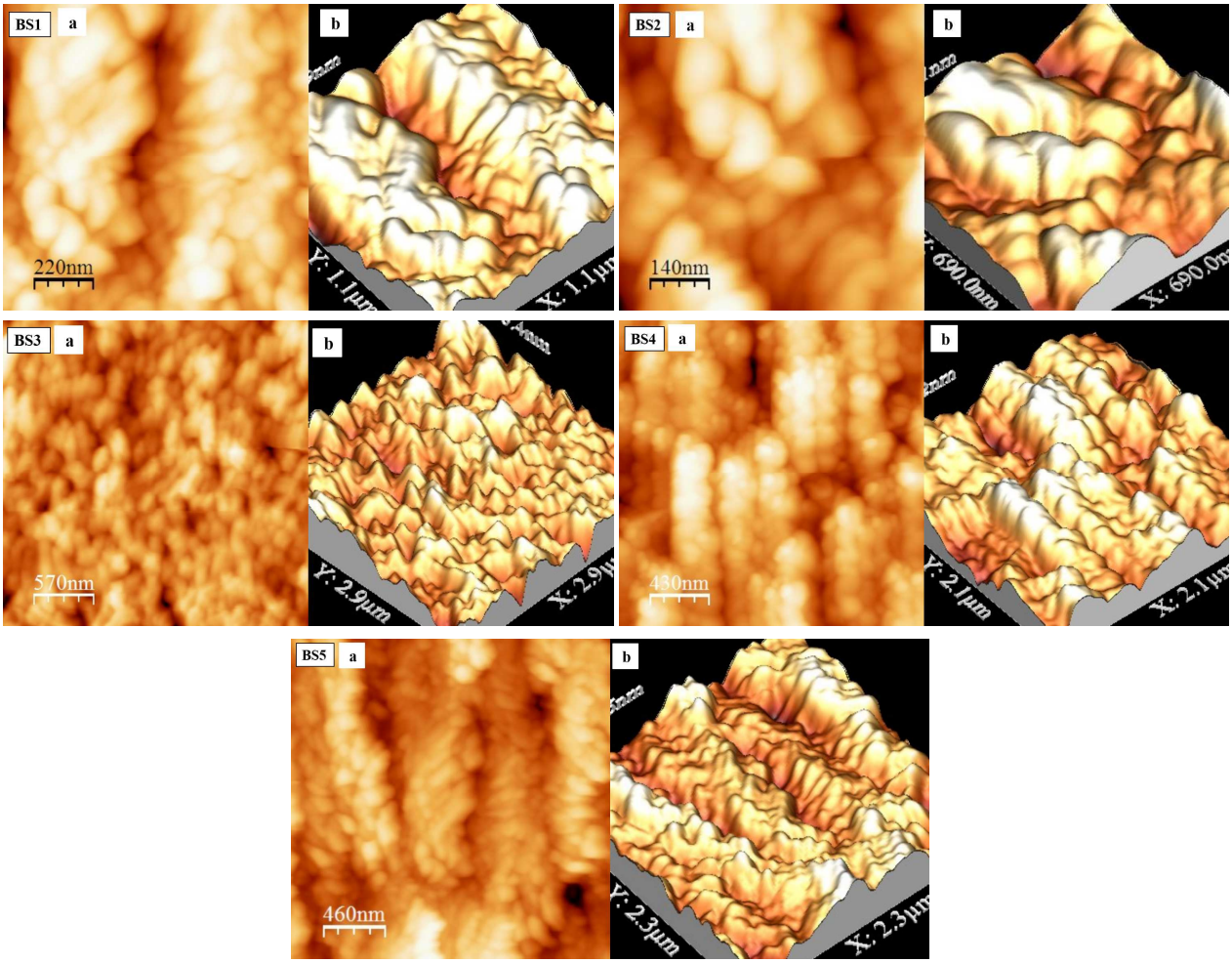

Fig. 6 Atomic force microscopy (AFM) images of $Bi_2(S_{1-x}Se_x)_3$(BS1 to BS5) thin Films

3.5 Optical absorption studies

Fig.7 (a) shows optical absorption spectra of $Bi_2(S_{1-x}Se_x)_3$ thin films recorded using UV-Vis spectrophotometer in wavelength range 400-1100 nm. Fig.7 (a) clearly shows that maximum optical absorption observed around 700-900 nm. There is an overall increase in absorption seen as the thickness of the film increases from samples BS1 to BS5. The fundamental absorption, which corresponds to electron excitation from the valance band to conduction band, can be used to determine value of optical band gap by using following equation 5.[32]

$$\alpha = \frac{A(h\nu - Eg)^n}{h\nu} \qquad [5]$$

where, 'A' is a parameter depends on transition probability, *h* is Planck constant, *'Eg'* is the optical band gap energy of material, and exponent '*n*' depends on type of transition. The values of *'n'* for direct allowed, indirect allowed, direct forbidden and indirect forbidden transition are 1/2, 2, 3/2 and 3, respectively.

Optical band gap energy values of $Bi_2(S_{1-x}Se_x)_3$ thin films were obtained by plotting graph of $(\alpha h\vartheta)^2$ *vs.* photon energy ($h\vartheta$), as shown in fig 7 (b). Linear nature of plot suggests direct and allowed type of transition. The band gap energy is decreased from 1.69 to 1.43 eV. The optical band gap values are well in agreement with reported values[33-36]. These obtained band gap energies are summarized in Table 1. From optical absorption study, it is seen that red shift is observed in band gap with increase in Se content.

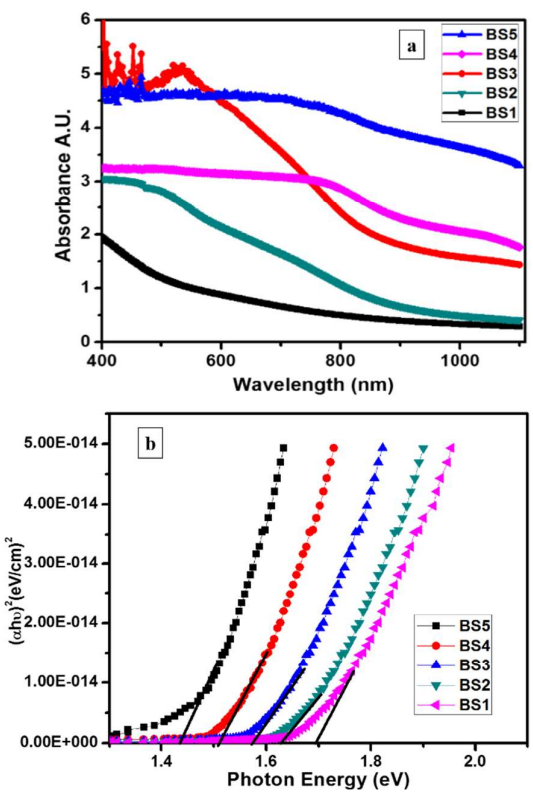

Fig.7 (a) Optical absorption spectra of $Bi_2(S_{1-x}Se_x)_3$(BS1 to BS5) thin films, **(b)** Plots of $(\alpha h\upsilon)^2$ (eV/cm)^2 vs. photon energy (eV) of $Bi_2(S_{1-x}Se_x)_3$(BS1 to BS5) thin films.

3.6 Photo electrochemical (PEC) properties

PEC performance of $Bi_2(S_{1-x}Se_x)_3$ thin films was checked with the help of a standard two electrode configuration. Fig 9 shows *J–V* curves of PEC cells formed by $Bi_2(S_{1-x}Se_x)_3$ thin films as working electrode (active surface area 1 cm^2) and graphite (G) as counter electrode, under illumination of light using 100 W halogen lamp in 0.5 M iodite/ polyiodite redox electrolyte. The photo response of all samples was recorded after forming following cell configuration,

Glass/FTO/$Bi_2(S_{1-x}Se_x)_3$/iodite/polyiodite/Graphite

If photocurrent enhancement occurs in positive potential region it indicates that the material is *n*-type semiconductor.[37,38] From, *J–V* curves it was revealed that photocurrent enhancement observed in positive potential region, thus confirming that $Bi_2(S_{1-x}Se_x)_3$ is *n*-type semiconductor.

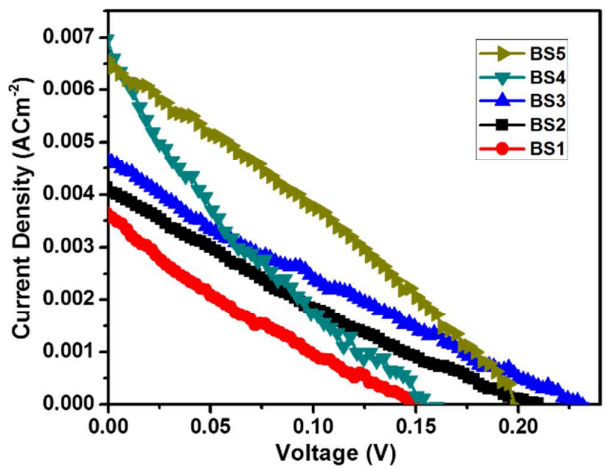

Fig. 9 *J-V* characteristics of $Bi_2(S_{1-x}Se_x)_3$ (BS1 to BS5) thin films

Output parameters of PEC solar cell, i.e. light conversion efficiency (η %) and fill factor (FF) are calculated from equations (6) and (7), respectively[14]

$$\eta\,\% = \frac{Jsc \times Voc}{Pin} \times FF \times 100 \qquad (6)$$

$$FF = \frac{Jmax \times Vmax}{Jsc \times Voc} \qquad (7)$$

where, P_{in} is the input light intensity, J_{sc} is the short circuit current density and V_{oc} is the open circuit voltage. J_{max} and V_{max} are the values of maximum short circuit current density and maximum open circuit voltage respectively, which is extracted from an output characteristic of the PEC cell.

Series resistance (R_s) and shunt resistance (R_{sh}) of all samples were estimated from the inverse of the slope of the *J–V* curves using equations (8) and (9),

$$\left[\frac{dI}{dV}\right]_{I=0} \approx \frac{1}{R_s} \qquad (8)$$

$$\left[\frac{dI}{dV}\right]_{V=0} \approx \frac{1}{R_{sh}} \quad (9)$$

The compact and densely packed $Bi_2(S_{1-x}Se_x)_3$ thin films can absorb sufficient light and generate electrons. These photo generated electrons can transport directly through nano structured compact layers to the conducting substrates. The output parameters of PEC cell such as, fill factor (FF), conversion efficiency (η %), series resistance (Rs) and shunt resistance (Rsh) were tabulated in Table 3.

Table 3 Solar cell parameters of $Bi_2(S_{1-x}Se_x)_3$ thin films

Sample code	Jsc (A/cm^2)	Voc (V)	Jmax (A/cm^2)	Vmax (V)	Rs Ω	Rsh Ω	Fill Factor (FF)	Conversion efficiency (η) %
BS1	0.00403	0.2097	0.00208	0.0887	547	6875	0.2192	0.1852
BS2	0.00667	0.1534	0.00275	0.0763	459	5986	0.2277	0.2103
BS3	0.00463	0.2290	0.00213	0.1177	367	4587	0.2373	0.2516
BS4	0.00485	0.1903	0.00233	0.1226	257	3587	0.3097	0.2859
BS5	0.00644	0.1952	0.00384	0.1052	194	1523	0.3158	0.3845

From Table 3 it is observed that samples BS5 show better performance as compared to BS1 to BS4. As observed from structural and morphological studies, samples BS1 to BS4 have lower crystallites sizes giving rise to higher dislocation density and higher micro strain which leads to more loss mechanisms in the photo electrode. They have recombination problems due to the existence of considerable grain boundaries in the film. Therefore the electron trapping at the surface and inter grain boundaries result in lower light conversion efficiency.[39,40] Samples BS5 have larger surface area and lower dislocation density which leads to reduced grain boundaries. This significantly reduces the recombination losses of photo generated charge carriers due to decrement in grain boundary resistance. They also have increased pore size as well as short nanoflakes with thin petals of marigold like surface morphology which is advantageous for exposing a larger effective surface area for light absorption. They also can provide a direct pathway for electron transport through interconnected fibers and petals much faster than in nanoparticles and nanoflakes with marigold like structure[41, 42] as shown in fig. 10a–c.

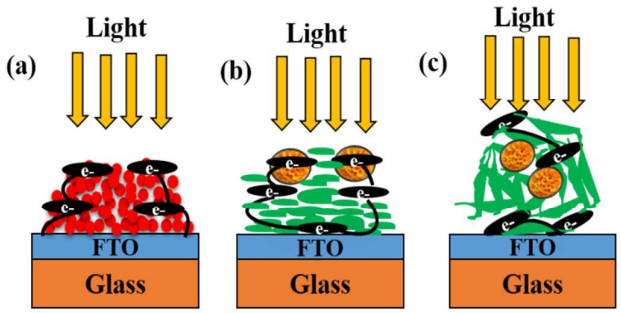

Fig. 10 Comparative representation of electron transfer of $Bi_2(S_{1-x}Se_x)_3$ thin film a) Nanoparticles b) Nanoflakes + Merigold like structure c) Short Nanoflakes + Framework of thin petals of Merigold like structure

Also, when the photons are incident on the framework of thin petals, the pores created by interconnection are favorable for the establishment of an intimate contact between an electrolyte and interconnected framework of thin petals leads to fast removal of holes permitting electrons to transfer through several crystallites with little probability of their recombination in the PEC system.[43] Hence it is concluded that increased light conversion efficiency of Bi_2Se_3 may be due to the increased effective surface area for light absorption, lower dislocation density, micro strain and lower density of grain boundaries in the electron transport than in nanoflakes with marigold like structure $Bi_2(S_{0.5}Se_{0.5})_3$ and nanosphered Bi_2S_3 thin film.

Conclusions

Nanostructured $Bi_2(S_{1-x}Se_x)_3$ thin films were successfully deposited on glass and FTO-coated glass substrate by simple CBD at room temperature (300K). From XRD analysis, synthesis of nanocrystalline $Bi_2(S_{1-x}Se_x)_3$ with orthorhombic crystal structure was confirmed. The dislocation density and micro-strain were found to decrease from sample BS1 to BS5 and crystallite size increased with increase in Se content in the films. Very interesting changes in morphology were observed as Sulpher was replaced by Selenium in the films. In BS1 well defined tightly packed nano particles were observed whereas in BS5 composite structure of thin walled nanoflowers along with nano sized flakes was observed. It was seen that morphology observed in BS5 is beneficial for effective increase in photocurrent and efficiency of photoelectrochemical solar cell. Band gap energy changed from 1.69 to 1.43 eV with increase in selenium content in the films. Highest conversion efficiency obtained was 0.3845 % for Bi_2Se_3 thin films. These might be due to low values of R_s and reduced grain boundaries resistance. These results promise the effective application of $Bi_2(S_{1-x}Se_x)_3$ thin films to be utilized for enhancement in light harvesting efficiency.

Acknowledgements

The author would like to thank Vice-Chancellor of DIAT, Pune for extending all the facilities of the institute. Authors acknowledge financial support from DRDO-DIAT Program on Nano Materials from ER-IPR of Defence Research and Development Organization.

Notes and references

aThin Film Material Laboratory, Department of Applied Physics, Defense Institute of Advance Technology (DU), Girinagar, Pune-411025, India
bMaterials Research Laboratory, Department of Chemistry, Shivaji University, Kolhapur-416004, India.
Corresponding author: tejashreebhave@diat.ac.in (T. M. Bhave)
Tel: +91 20 2430 4093; Fax: +91 20 2438950

1 C. M. Huang, L. C. Chen, G. T. Pan, T. C. K. Yang, W. S. Chang and K. W. Cheng, *Mater. Chem. Phys.,* 2009, **117**, 156.
2 S. S. Mali, S. K. Desai, D. S. Dalavi, C. A. Betty, P. N. Bhosale and P. S. Patil, *Photochem. Photobiol. Sci.,* 2011, **10**, 1652.
3 S.S. Mali, C.A. Betty, P.N. Bhosale, P.S. Patil, *Electrochim. Acta* 2012, **59** 113.
4 Z. Zang, A. Nakamura, J. Temmyo, *Opt. Express,* 2013, **21** 11448.
5 Z. Zang, A. Nakamura, J. Temmyo, *Mater. Lett.,* 2013, **92**, 188.
6 C.D. Lokhande, A. U. Ubale and P.S. Patil, *Thin Solid Films,* 1997, **302**, 1.
7 H. Moreno-Garcia, M. T. S. Nair and P. K. Nair, *Thin Solid Films*, 2011, **519**, 7364.
8 B. R. Sankapal and C. D. Lokhande, *Materials Chemistry and Physics,* 2002, **73**, 151.
9 A. A. Tahir, M. A. Ehsan, M. Mazhar, K. G. Upul Wijayantha, M. Zeller and A. D. Hunter, *Chem. Mater,* 2010, **22**, 5084.
10 B. R. Sankapal and C. D. Lokhande, *Solar Energy materials and Solar Cell,* 2001, **69**, 43.
11 A. R. Patil, V. N. Patil, L. P. Deshmukh and P. N. Bhosale, *Materials Chemistry and Physics*, 2000, **65**, 266.
12 S. M. Patil, S. R. Mane, R. M. Mane, S. S. Mali, P. S. Patil and P. N. Bhosale, *Can. J. Chem.,* 2011, **89**, 1375.
13 R. K. Mane, B. D. Ajalkar and P. N. Bhosale, Materials Chemistry and Physics, 2003, **82**, 534.
14 N. B. Pawar, S. S. Mali, M. M. Salunkhe, R. M. Mane, P. S. Patil and P. N. Bhosale, New J. Chem, 2012, 36, 1807.
15 N. B. Pawar, S. S. Mali, S. D. Kharade, M. G. Gang, P. S. Patil, J. H. Kim, C. K. Hong, P. N. Bhosale, Current Applied Physics, 2014, 14, 508.
16 S. D. Kharade, N. B. Pawar, S. S. Mali, C. K. Hong, P. S. Patil, M. G. Gang J. H. Kim, P. N. Bhosale, J. Mater. Sci. 2013, 48, 7300.
17 Manauti M. Salunkhe, Kishorkumar V. Khot, Pramod S. Patil, Tejashree M. Bhave and Popatrao N. Bhosale, *New Journal of Chemistry*, DOI: 10.1039/c4nj01790k
18 B. Pajova, and I. Grozdanov, *Thin solid films*, 2002, **408**, 6.
19 R. M. Mane, S. R. Mane, R. R. Kharade and P. N. Bhosale, *J. Alloys. Compd.,* 2011, **491**, 321.
20 R. Herberholz, M. J. Carter, *Solar Energy Mater. Sol. Cells,* 1996, 441, 357.
21 S. D. Kharade, N. B. Pawar, V. B. Ghanwat, S. S. Mali, W. R. Bae, P. S. Patil, C. K. Hong, J. H. Kim and P. N. Bhosale, *New J. Chem*, 2013, **37**, 2821.
22 S. Min, O. Joo, R. S. Mane, K. Jung, C. D. Lokhande and S. Han, *Photochem. Photobiol. A*, 2007, **187**, 133.
23 R. P. Pratap, R. W. Miles, K. T. Ramkrishna Reddy, *Sol. Energy Mater. Solar Cells*, 2010, **94**, 148.
24 T. Kameyama, T. Osaki, K. Osaki, K. Okazaki, T. Shibayama, *J. Mater. Chem.,* 2010, **20**, 5319.
25 K. V. Khot, S. S. Mali, N. B. Pawar, R. M. Mane, V. V. Kondalkar, V. B. Ghanwat, P. S. Patil, C. K. Hong, J. H. Kim, J. Heo and P. N. Bhosale, *Mater. Sci: Mater. Electron.*, 2014, **25**, 3762.
26 V. Pal, D. Samantha, S. Oehorai, A. K. Chaudhari, *J. Appl. Phys.*, 1993, **74**, 6368.
27 J. Horak, K. Cermark, L. Koudelkar, *J. Phys. Chem. Sol.,* 1886, **47**, 805.
28 L. J. Horak, L. Koudelkar, *J. Phys. Stat. Sol. A.,* 1984, **84,** 143.
29 I. Pupitasari, T. P. Gujar, K. Jung, O. Joo, *J. Mater. Process Technol* , 2008, **201**, 775.
30 P. Pai, G. Zhang, Y. Chen, H. Jiang, Z. Feng, Z. Lin, J. Zhan, *Chem. Commun,* 2012, **48**, 3006.
31 H. Khallat, G. Chai, O. Lupan, L. Chow, S. Park, A. Schulte, *Appl. Surf. Sci.,* 2009, **255**, 4129.
32 S. S. Mali, P. S. Patil and C. K. Hong, *ACS Appl. Mater. Interfaces,* 2014, **6**, 1688.
33 Z. P. Lui, J. B. Liang, S. Li, S. Peng and Y. T. Qian, *Chem-Eur. J.*, 2004, **10**, 6314.
34 Z. Kebbab, N. Benramdane, M. Medles, A. Bouzidi, H. Tabet-Derraz, *Solar Energy Materials and Solar Cells*, 2002, **71**, 449.
35 X. Yang, X. Wang and Z. Zhang, *J. Cryst. Growth,* 2005, **276**, 566.
36 S. K. Mishra, S. Satpathy and O. Jepsen, *J. Phys, Condens Matter*, 1997, **9**, 461 .
37 S.B. Ambade, R.S. Mane, S.S. Kale, S.H. Sonawane, A.V. Shaikh, S.H. Han, *Appl. Surf. Sci.* 2006, **253**, 2123.
38 S.S. Hongmei, Y. Gao, D. Qin, J. Chen, *J. Mater. Chem.,* 2012, **22**, 19207.
39 R. S. Mane, B. R. Sankapal and C. D. Lokhande, *Mater. Chem. Phys.,* 1999, **60**, 196.
40 V. D. Das and P. G. Ganesan, *Mater. Chem. Phys.,* 1998, **57**, 57.
41 F. Amano, D. Li and B. Ohtani, *ECS Trans.,* 2010, **28**, 127.
42 Q. Zhang and G. Cao, *Nano Today*, 2011, **6**, 91.
43 G. Hodes, I. D. J. Howell and L. M. Peter, *J. Electrochem. Soc.,* 1992, **139**, 3136.

Low temperature and controlled synthesis of $Bi_2(S_{1-x}Se_x)_3$ thin films using simple chemical route:Effect of bath composition

Manauti Salunkhe[a], Kishorkumar V. Khot[b], Sanjay H. Sahare[a], Popatrao N. Bhosale[b] and Tejashree M. Bhave[a*]

aThin Film Material Laboratory, Department of Applied Physics, Defense Institute of Advance Technology (DU), Girinagar, Pune-411025, India
bMaterials Research Laboratory, Department of Chemistry, Shivaji University, Kolhapur-416004, India.
Corresponding author: tejashreebhave@diat.ac.in (T. M. Bhave)
Tel: +91 20 2430 4093; Fax: +91 20 2438950

Graphical Abstract

Simple room temperature chemical route, Ternary $Bi_2(SSe)_3$ thin films, Nanocrystalline material, Porous surface morphology, Photoelectrochemical response.